Received: 10 April 2025 | Revised: 4 June 2026 | Accepted: 17 June 2026

DOI: 10.1002/esp.70351

RESEARCH ARTICLE

ESPL WILEY

Holistic analysis of shoreline change and mudbank dynamics across the Guiana coastline

Martin S. J. Rogers[1,2] | **Tom Spencer**[2]

[1]British Antarctic Survey, Cambridge, UK

[2]Department of Geography, University of Cambridge, Cambridge, UK

Correspondence
Martin S. J. Rogers, British Antarctic Survey, Cambridge, UK.
Email: marrog@bas.ac.uk

Funding information
Natural Environment Research Council, Grant/Award Numbers: NE/M009009/1, NE/R011265/1

Abstract

The Guiana coastline, stretching for 1500 km between the Amazon and Orinoco Rivers in South America, is one of the most dynamic shorelines in the world. The shoreline is characterised by alongshore migratory, shore-attached mudbanks, with shoreline accretion and mangrove colonisation during in-bank periods, followed by significant shoreline erosion during interbank phases. While considerable research has been undertaken along the Guiana coastline, not all analyses have used sufficiently long temporal sequences of imagery to track at least one complete accretion–erosion cycle and analysis has often been limited to a localised region. To address these concerns, this paper provides the first ever analysis of shoreline change across the entire Guiana coastline annually over a 35-year period (1988–2023). Using the seaward extent of mangrove forest extracted from Landsat multispectral satellite imagery as a proxy for shoreline position, annual rates of shoreline change were measured at 200-m intervals along the 1500-km shoreline, providing new insights into the evolution of the entire shoreline system. This analysis identified nine mudbanks migrating alongshore at rates of between 0.26 and 1.38 km year^{-1}, lower than previously cited values of 0.9–5 km year^{-1}. These lower rates challenge the traditionally accepted 30-year oscillatory model for this coastline, instead suggesting a minimum 40-year minimum periodicity. Furthermore, and also contrary to previous research, this analysis identified no evidence of a cycle in shoreline accretion—erosion across two extensive regions of the Guiana coastline: Saramacca in Suriname and the entire coastline of Guyana. In these locations, other landforms affected shoreline position: naturally migrating headlands, emplaced polders and sites of rapid accretion along anthropogenically modified coastlines. Correlation analysis was conducted between shoreline change metrics, wave metrics and climate indices including the North Atlantic Oscillation and the El Niño Southern Oscillation. At the landform scale, significant wave height and direction had the strongest statistical relationship with shoreline change. These findings revise understanding of mudbank-driven shoreline dynamics and highlight the need for long-term observations for coastal monitoring and management.

KEYWORDS
coastal erosion, Google Earth Engine, Guiana, mangrove dynamics, satellite imagery

1 | INTRODUCTION

Mangrove forests have been shown to play important roles in coastal protection (Menéndez et al., 2020), climate change mitigation through carbon storage (Rovai et al., 2018), improving biodiversity and fisheries enhancement (Zu Ermgassen et al., 2020) and supporting community livelihoods and well-being (Sievers et al., 2023). There is, therefore, considerable interest in monitoring mangrove dynamics to identify mangrove losses driven by anthropogenic actions, increasing the legal protection of remaining mangrove areas and restoring areas where mangroves have been lost (Veverka et al., 2025).

Mangroves have been shown to be opportunistic colonisers of surfaces relatively high in the tidal frame, generated by local hydrodynamic forcing and associated sediment transport and deposition (Friess & McKee, 2021; Swales et al., 2015; Thom, 1967). Shallow marine settings are thus often characterised by extensive intertidal mudflats commonly accompanied by equally extensive mangrove forests. Migratory mudflats are found in West Papua and Makassar Strait, Indonesia, and the Gulf of Papua, Papua New Guinea; (Proisy et al., 2021), the Kerala coast, India; the Yellow River delta, Bohai Sea of China (Zhu et al., 2024); the Guiana's coastline in South America; and in Florida Bay, United States (Best et al., 2025). In these locations, patterns of wave energy dissipation drive changing foci of sediment accretion and erosion and accompanying patterns of mangrove extension and loss. Better determining the dynamics of these linked unvegetated and vegetated systems around the world is essential, not least in the context of better predicting the impacts on them of near-future accelerated sea level rise (Fox-Kemper et al., 2021) and potential changes in ocean-margin storminess (Seneviratne et al., 2021).

The Guiana coastline, stretching for 1500 km along the northeastern coastline of South America between the Amazon and Orinoco Rivers, is one of the most dynamic shorelines in the world. The shoreline is characterised by a massive northwesterly conveyor belt of fine-grained sediments, redistributing 15%–20% of the Amazon River sediment discharge (Anthony et al., 2014), and organised into a series of 20–25 large-scale (wavelengths of 10- to 60-km alongshore, widths of 30- to 40-km cross-shore and maximum sediment thicknesses of 5–10 m; Augustinus, 2004; Froidefond et al., 1988), migratory, shore-attached mudbanks. The individual banks are separated by 10- to 40-km-long interbank sections (Allison et al., 2000). In the 'bank' phase, lee-side locations are characterised by fluid muds measuring 1 m or more in thickness (Lefebvre et al., 2004). Resultant mud damping can reduce incident wave energy by 85%–90% (Best et al., 2022; Winterwerp et al., 2007). The gel-like fluid mud deposits are pushed shoreward over the neap-spring cycle, aided by transport under solitary waves (Gardel et al., 2011; Gratiot et al., 2007) and form distinct bar-like accumulation features. Extensive colonisation of these bank surfaces by mangroves follows sediment dewatering and consolidation, driven by periods of low tide exposure of muds; in particular, the development of desiccation cracks is critical because these allow the trapping of propagules of *Avicenna germinans* (Fiot & Gratiot, 2006). Mangrove colonisation begins on topographic highs but then rapidly extends to cover the entire mudflat, giving an additional dissipation of remaining wave energy of 15% within the first 120 m of the mangrove belt (Best et al., 2022; Toorman et al., 2018). The trailing updrift margins of the banks, and the developing interbank areas, are characterised by erosion of the now compacted mudbank silt-clays, mangrove forest collapse and loss and shoreline retreat, often at very rapid rates (Fromard et al., 2004). A commonly accepted 30-year oscillatory model has been used to characterise the frequency of these dynamics at individual localities (Anthony et al., 2010; Anthony et al., 2014; Fromard et al., 2004).

A considerable body of research has been undertaken along the coastline of the Guianas over the last 40 years, with increasing levels of technical sophistication and improved resolution of both temporal and spatial scales of image acquisition and analysis, now enhanced by the availability of web-based platforms, such as Google Earth Engine (Gorelick et al., 2017), to analyse large volumes of satellite imagery and engage with a number of shoreline-mapping algorithms (e.g., Rogers et al., 2021; Vos et al., 2023). These studies have estimated that the banks of the Guiana coast are currently migrating alongshore at rates of between 0.9 and 1.0 (Abascal-Zorrilla et al., 2024; Froidefond et al., 1988) to > 5 km $year^{-1}$ (Gardel & Gratiot, 2005). However, few analyses have used sufficiently long temporal sequences of imagery to track at least one complete cycle of bank and interbank shoreline change. And where high temporal coverage has been achieved, the analysis is often limited to a localised region or has been defined by reference to nation state boundaries, which have no physical meaning in the presence of migratory natural systems. Furthermore, some recent analyses (e.g. De Vries et al., 2022) have shown that the coastline of the Guianas shows greater local complexity than can be explained by a simple cyclicity of bank v. interbank presence; coastal erosion can still occur when mudbanks are present and accretion can take place in their absence. Finally, all these natural processes are overlain by human interventions at the coast which, to varying degrees, impact and modify the natural bio-physical systems (Brunier et al., 2019; Proisy et al., 2021).

From an analysis of SPOT imagery, Gardel & Gratiot (2006) show that on geomorphological timescales, there is a relatively short interval (2.5 years or less) between the maximum development of a new mudbank and the initiation of mangrove colonisation; once colonisation starts, it rapidly spreads to cover the entire bank (90% coverage in 3 years; Gensac et al., 2011) and leads to the development of a tall forest (Lefebvre et al., 2004; Proisy et al., 2009). It can reasonably be argued, therefore, that the presence/absence of mangrove cover, readily seen in sequential remote sensing imagery, provides a reliable proxy of shoreline position. Mapping of mangrove ecology within medium-resolution satellite imagery of this region is also aided by the relatively low diversity of mangrove forests. The formative phase of vegetation establishment is dominated by *Avicennia germinans* with locally *Laguncularia racemosa;* eroding mangrove forests consist almost entirely of *A. germinans* (Fromard et al., 2004).

In this paper, we apply image thresholding techniques to a 35-year record of multispectral imagery from the Landsat satellite platforms to capture changing shoreline position, spanning the entire Guiana coastline. We establish new rates of alongshore migratory behaviour and test the widely accepted model of a 30-year cycle to bank/nonbank presence by identifying differences in mudbank migration speed and form across the entire Guiana coastline.

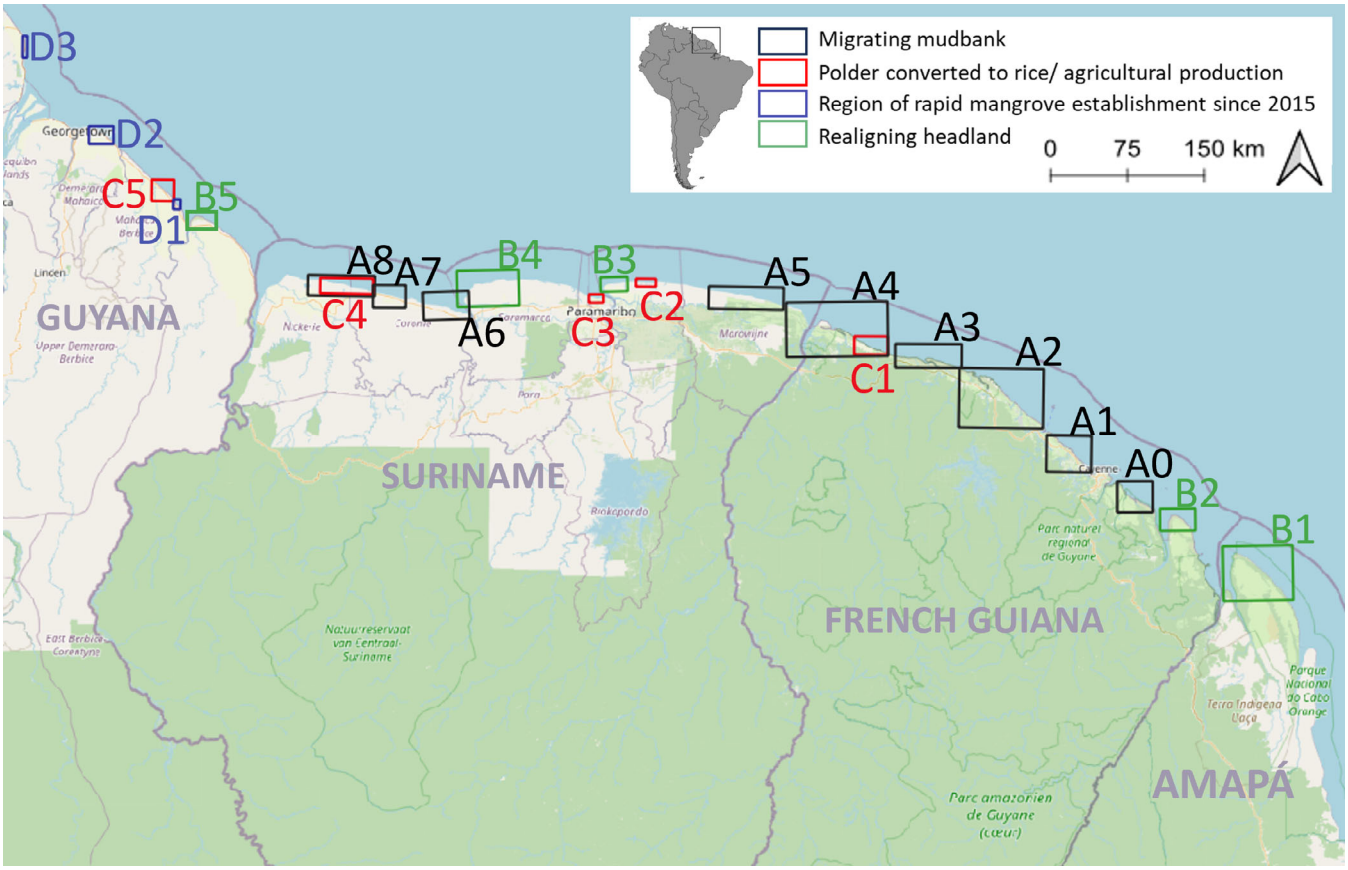

FIGURE 1 Location of profiles identified along the Guiana coastline. See Figure 3 for characteristic forms of the profiles and Appendix S1 for zoomed in representations of all identified coastlines and coastal landforms.

2 | MATERIALS AND METHODS

2.1 | Study site and remote sensing datasets

The Guiana coastline, situated between the mouths of the Amazon and Orinoco Rivers (8.120°N, −59.12°E and 2.425°N, −50.76°E), contains the coastlines of the countries of Guyana and Suriname, the territory of French Guiana and the region of the River Uaçá in Amapá, the northernmost state of Brazil (Figure 1).

Datasets were derived from NASA's Landsat missions 5, 7 and 8, which capture multispectral satellite imagery at 30-m spatial resolution for the period 1988–2023 from the Google Earth Engine (GEE) repository. Ortho-rectified and geo-registered Tier 1 data were selected, enabling imagery from the different Landsat missions to be compared. Some Landsat 5 imagery was available since its launch in 1984; however, coverage across the study area between 1984 and 1987 was very limited, so this study only used this imagery from 1988 onwards. The northernmost 160 km of Amapá and westernmost 120 km of the Guyana coastline were omitted from this study due to very low satellite image availability in GEE for this region prior to 2013. To reduce the impact of cloud cover on shoreline detection, the Guiana coastline was separated into 16 subset regions (Appendix S1), and the Landsat scene with the lowest cloud cover for each region was selected.

Where imagery was available, one image was collated for each calendar year between 1988 and 2023, resulting in a minimum of 29 images being acquired at all 18 regions across the 33 years of this study. The only exception to this was the state of Amapá, northern Brazil, where only 20 images were available. To ensure consistency between regions, > 90% of the images were captured between June and September of each year. The months of June–September were prioritised because significant wave heights and associated rates of mudbank migration have been shown to be lowest in this period (Gratiot et al., 2007), mitigating the effects of inconsistencies in date when images were acquired. However, image availability, cloud cover and the scan-line corrector failure on the Landsat 7 sensor (de Jong et al., 2021) meant imagery was not captured at each region every year, and some images were acquired outside of the June–September window. In total, this study acquired and analysed a total of 535 cropped Landsat scenes.

To validate the accuracy of the shorelines derived using Landsat imagery, shoreline positions were also extracted from 3-m resolution PlanetScope satellites (PlanetLabs, 2023), acquired from the Planet repository and downloaded under an academic licence. Shoreline position was validated during three different years (2016, 2020 and 2023) at five test locations (Appendix S2), resulting in a total of 15 validation images. Test locations covered a range of shoreline settings along the Guiana Coastline, including open coast migrating mudbanks (Sinnamary, French Guyana: Wia-Wia Nature Reserve, Suriname), rice polder (Mana, French Guiana), a headland (Posto Uaça, Brazil) and two stretches of coastline that contained a sea wall (Anna Regina and Georgetown, Guyana). Due to the dynamic nature of the mangrove position, Planet imagery was only used for validation if it was acquired within 2 weeks either side of the corresponding Landsat image. The

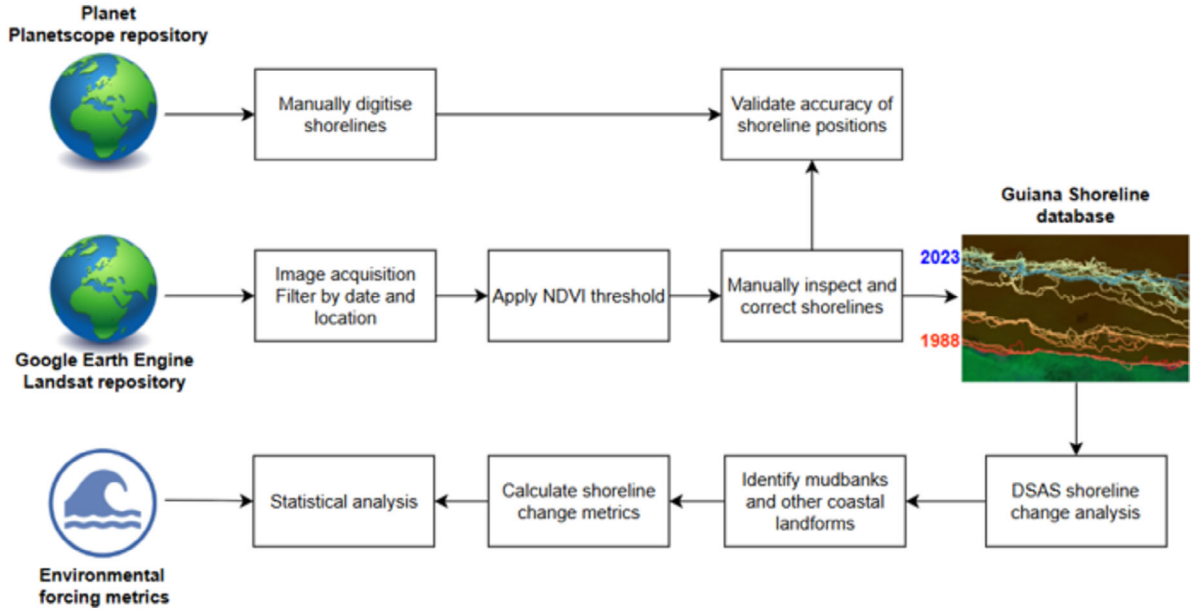

FIGURE 2 Data acquisition, image processing and shoreline evaluation steps carried out in this study.

remote nature and vast extent of the Guiana coastline precluded the use of *in situ* measurements for the validation process.

Despite the superior spatial resolution of Planet imagery, this imagery was not used for shoreline change detection due to its relatively short temporal coverage (2010 to present) and the geometric and radiometric heterogeneity in the images captured by the different satellite sensors within Planet Labs' satellite constellation (Saunier, 2021). Figure 2 provides an overview of all data acquisition and analysis steps employed in this study.

2.2 | Shoreline detection

Shoreline position was defined as the seaward extent of continuous mangrove vegetation cover. In locations where mangroves did not exist, for example in urban and polder regions, the seaward extent of other continuous vegetation types was used as the shoreline proxy. Isolated vegetation located seaward of the continuous vegetation cover, for example, small patches of early colonising mangrove, mudflat covered biofilms and aquatic vegetation, were not used in this analysis as they tend to reflect ecological than coastal geomorphological processes (Boak & Turner, 2005). Mangrove forests are primarily located between mean sea level and high tide elevations (Ellison, 2009). The relative stable position of seaward mangrove margins compared with, for example, shifting tidal flats means that the instantaneous waterline and diurnal tidal location was not considered during image selection.

Shoreline position was derived using the normalised difference vegetation index (NDVI):

$$NDVI = \frac{NIR - R}{NIR + R} \quad (1)$$

where NIR and R correspond to the near-infrared and red spectral bands, respectively (Kriegler et al., 1969). NDVI was used in this study because all mangrove species can be discriminated using the visible and near infrared wavebands (Tran et al., 2022). To ascertain the best NDVI threshold value to use, shorelines were generated using the ratio values {0.01, 0.1, 0.2, 0.3, 0.4}. Shoreline positions were compared to the shorelines generated by manually digitising the corresponding PlanetScope imagery (validation shorelines). The distance between the PlanetScope validation lines and NDVI threshold lines was at a minimum when using a threshold value of 0.3 (Appendix S2); this value was therefore applied to the NDVI images to generate a binary vegetated- non-vegetated land cover mask. This threshold value is consistent with that used in multiple other mangrove ecology studies (Satyanarayana et al., 2011; Le et al., 2020; Tran et al., 2022).

The land cover masks were polygonised using the Python coding library, GDAL, to generate coastal vegetation lines. The threshold method also generated polylines in other locations, for example, where an inland water body or inland cloud cover existed. To overcome this issue, any polyline containing an area corresponding to a ring contour was removed. All vegetation lines were subsequently manually inspected and corrected in locations where cloud occluded the shoreline position or where the shoreline erroneously reflected the position of isolated areas of vegetation, located seaward of the continuous vegetation cover. To identify the shoreline position in these locations, shorelines from previous and subsequent years were referred to.

2.3 | Shoreline change analysis

Shoreline change analysis was conducted using the ArcGIS plugin Digital Shoreline Analysis System (DSAS) (Thieler et al., 2009). At each transect, net shoreline change (NSC), defined as the relative position of the shoreline in 2023 compared with 1988 (Equation (2)), and absolute shoreline change (ASC), the cumulative magnitude of shoreline movement across all years, irrespective of its direction (Equation (3)), were calculated.

$$NSC = \sum_{t=0}^{t} d_t - d_{t-1} \quad (2)$$

$$ASC = \sum_{t=0}^{t} |d_t - d_{t-1}| \quad (3)$$

where $|d_t - d_{t-1}|$ corresponds to the magnitude of the distance between the shoreline at year, t, and previous year, $t - 1$. Concretely, a near-zero NSC but very large ASC value could be recorded at a transect where the shoreline has experience large-scale erosion and accretion of equal magnitude.

In addition, relative position to mean (RPM) was calculated as the shoreline position each year relative to the per-transect shoreline mean position (Equation (4)):

$$RPM = p_t - \overline{p} \quad (4)$$

where p_t corresponds to the shoreline position at year, t, and $\overline{p}$ is the mean shoreline position over the 36-year study period. A positive (negative) value corresponds to the shoreline being seaward (landward) of the mean position of the shoreline at that transect.

Shoreline metrics were calculated at a total of 5644 transects at 200-m intervals. This transect spacing was equal to or less than that used in analogous studies (Brunier et al., 2019; Walcker et al., 2015). The transects were subsequently manually inspected and removed where not orthogonal to the dominant shoreline direction, a problem which causes erroneously large NSC values. Transects were also removed in locations where migrating mudbanks caused deflections in river outlet direction, as these deflections led to anonymously large differences in shoreline position between successive years which did not reflect the alongshore mudbank migration.

To overcome years where imagery could not be collated, or where imagery was captured at different months each year, shoreline position was linearly interpolated to generate an additional variable corresponding to shoreline position on 1 June every year between 1988 and 2023. The date 1 June was chosen as this date (i) is outside the most active period of shoreline movement when seasonal trade winds along the coastline are at their strongest (Allison et al., 2000; Gratiot et al., 2007) and (ii) minimised the difference between the date of image acquisition each year and the interpolation date (> 90% images were acquired between June and September each year). All data points were populated into the Guiana shoreline database for subsequent analysis. The database is publicly accessible online (https://zenodo.org/records/15191879).

To quantify the uncertainty in shoreline position caused by this interpolation method, the shoreline was detected in an additional control image at the mudbank at Macouria, French Guiana; the rice polder at Mana, French Guiana; the migrating headland at Brammsprunt, Suriname; and the site of rapid mangrove development at Georgetown, Guiana. These images were acquired > 3 months apart from the nearest image at that site. The average difference between the interpolated and observed shoreline position across the four sites was 12.2 m, corresponding to subpixel differences in shoreline position caused by this interpolation method.

2.4 | Identifying different dynamics along the Guiana coastline

To understand the reasons for differences in NSC and ASC rates across the Guiana coastline, four different shoreline profile types were identified: (i) migrating mudbanks, (ii) natural headlands, (iii) emplaced rice or agricultural polders and (iv) sites of rapid accretion along anthropogenically modified coastlines (Figure 3). Headlands were identified if they were permanent features, differentiating them from temporary headlands which can deflect river outlets as mudbanks migrate over the site (Figure 3e,f). The presence of polders and structures orthogonal to the dominant shoreline direction was identified via manual inspection of satellite imagery. The positions of mudbanks were identified from the Guiana coastline database by identifying locations where NSC had transitions from being negative to positive when moving westwards along the shoreline. This corresponds to an area of net erosion being eastwards of an area of net accretion as a mangrove forest migrates westwards (Figure 3). The extent of each mudbank in transects was defined via subsequent manual inspection of the satellite imagery in each location.

2.5 | Shoreline change and environmental forcing metrics

To assess potential external forcing factors on shoreline change, data pertaining to wave conditions, mean sea level, the 18.6 nodal cycle as well as North Atlantic Oscillation and El Niño Southern Oscillation (ENSO) index values were obtained (Table 1). These metrics were selected because strong statistical relationships between these metrics and shoreline change values have previously been reported at individual sites (Orseau et al., 2020) or at a pan-Guiana scale (Gratiot et al., 2007), but no systematic review of the relationships at multiple scales has been conducted.

The wave parameters (significant wave height (H_s), mean wave period (T_m) and mean wave direction (θ_m)) were generated by the ERA5 ECMWF Ocean Wave Model (ECWAM). ECWAM describes the development, size and direction of wind-generated waves and is coupled to atmospheric and ocean models, providing wave parameter information at 0.5° resolution. All wave parameters, as well as mean and 95th percentile sea level data, were downloaded from the ERA5 data repository in .grib format (ECMWF, 2014).

The ECWAM dataset provides a near-continuous field of wave and sea level parameter values, spanning the entire Guiana coastline over the 33-year study period, enabling analysis with corresponding shoreline change data. It is recognised that there is high variability in the nearshore incident wave field due to its interaction with a complex nearshore bathymetry. Nevertheless, ECWAM data were used due to the paucity of *in situ* wave measurements, particularly any spanning close to the length of the 33-year shoreline change study.

Shoreline change was compared to three wave forcing variables previously identified as important drivers of alongshore movement of sediment (Komar & Inman, 1970): significant wave height, H_s; the ratio between H_s and T_m, R_w (Equation (5)); and the alongshore component of H_s, C_L (Equation (6)):

$$R_W = \frac{H_s^3}{T_m^2} \quad (5)$$

$$C_L = \frac{H_s^3}{T_m^2} \sin\alpha \cos\alpha \quad (6)$$

where α is the wave approach angle at the shoreline, calculated for every coastal landform as the angle between θ_m and the dominant

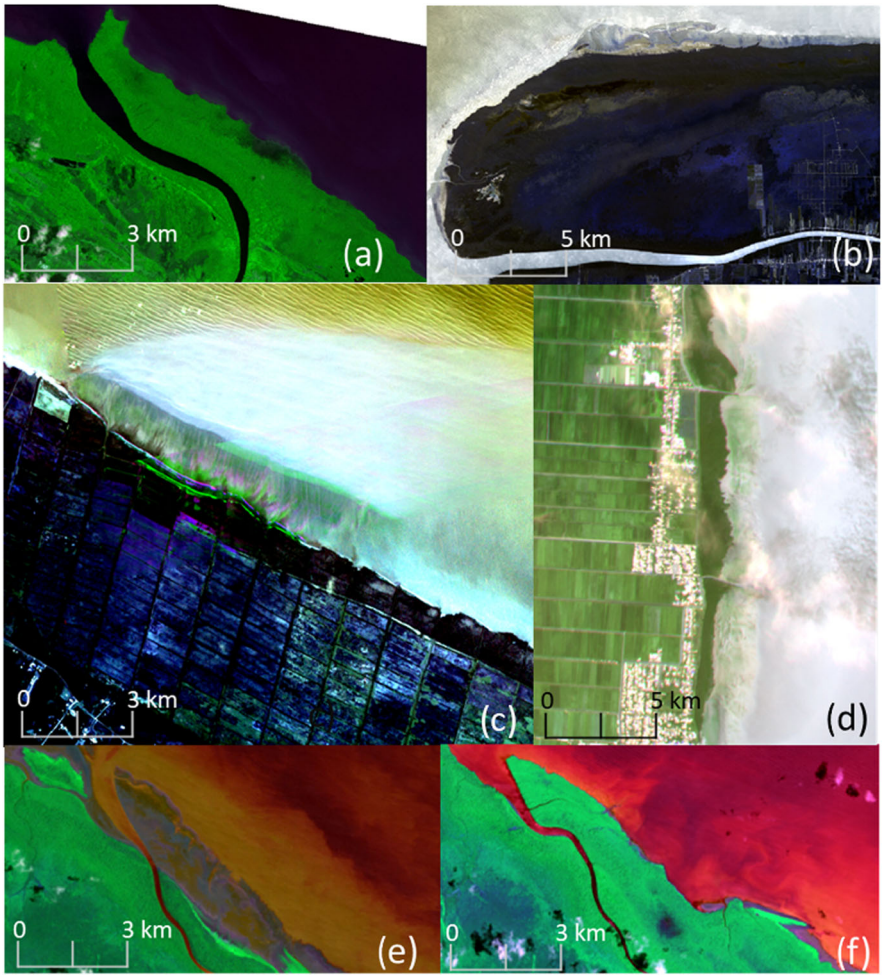

FIGURE 3 Examples of the different shoreline profiles: (a) migrating mudbank, Sinnamary, French Guiana; (b) permanent natural headland, Coppename nature reserve, Suriname; (c) rice polder, Mana, French Guiana; (d) site of rapid accretion, with groynes orthogonal to general shoreline orientation, anthropogenically modified coast, Anna Regina, Guyana; (e) and (f) temporary headland formed near Cayenne, French Guiana, with mudbank migrating over, and deflecting river Kaw. Images (a), to (d) and (f): Landsat 8; (d): planet satellite.

TABLE 1 External forcing factor metrics used, their spatial and temporal resolution and summary of preprocessing steps taken to harmonise these datasets with the annual shoreline change metrics.

External forcing factor	Metric	Temporal resolution	Spatial resolution	Postprocessing steps
Ocean waves	H_s: Significant wave height	Daily	25 km	Calculate mean value for previous winter (October–February).
Ocean waves	R_W: Wave height: wave period ratio (Equation (5))	Daily	25 km	Calculate mean value for previous winter (October–February).
Ocean waves	C_L: Alongshore component of H_s (Equation (6))	Daily	25 km	Calculate mean value for previous winter (October–February). Calculate per-pixel shoreline angle.
Mean sea level	Mean sea level	Annual	25 km	Calculate mean value across study area.
18.6 nodal cycle	Mean high water (MHW)	Annual	Single entry	Calculate MHW from prediction of tidal values.
NAO	October–March index	Monthly	Single entry	Predicted hourly values were converted to mean values for October–March
ENSO	Multivariate ENSO index version 2 (MEIV)	Bimonthly	Single entry	Calculate mean index value October–March

shoreline direction. The dominant shoreline direction was calculated using the angle measurer feature in QGIS. Wave metric values were calculated individually for each landform by identifying the ERA5 data pixels closest to each site. Only the wave values for the preceding winter months (November–February) were used; previous research has shown that the stronger wave conditions at this time of year coincide with the highest rates of mudbank mobilisation (Augustinus, 2004).

To investigate the teleconnection between shoreline dynamics and climate indices, the study used (i) the October to March North Atlantic Oscillation (ONDJFM NAO) index (NOAA, 2024a), for when the mudbanks are most mobile (Anthony et al., 2014; Gratiot et al., 2007) and (ii) the Mean ENSO Index Version 2 (MEIV) (NOAA, 2024b). To generate a time series of mean high water (MHW) from which to capture the 18.6-year nodal cycle, tide gauge data from the Ile Royale tide gauge near Cayenne were obtained from the Global

Extreme Sea Level Analysis (GESLA3) dataset (Haigh et al., 2023). Harmonics were extracted from hourly tidal data from 2018 to predict mean MHW between 1988 and 2023.

To determine the strength of statistical relationships, tests for correlation were conducted between NSC and ASC values and all external forcing factors. The Shapiro test for normality was applied to all datasets prior to conducting correlation tests. Pearson's correlation coefficient was used for normally distributed data, and Spearman's rank was applied to nonnormally distributed datasets (Dytham, 2011). For all tests, the null hypothesis was rejected when $p < 0.05$. To account for lags in the shoreline response to external forcing factors, lagged correlation analysis using a lag time of 1–3 years was also conducted.

3 | RESULTS

3.1 | Pan-Guiana spatial dynamics

The Guiana coastline can be split into three distinct sections characterised by their rates of ASC and NSC (Figure 4). The first section runs from north of the Amazon delta to the site of the formation of the most easterly, newest mudbank, A0, situated east of Cayenne, French Guiana (2.15°N, 50.65°W) to (4.70°N, 52.00°W). With the exception of the two realigning headlands, B1, Cabo Orange, and B2, Pointe Béhague, the coastline in this section has retreated every year since 1988 and ASC values do not exceed 2000 m. The second, central section contains all the active mudbanks, beginning at the lee side of mudbank A0, Cayenne, French Guiana, and ending at the front edge of A8, Totness, Suriname, and encompasses the coastlines of French Guiana and Suriname (4.70°N, 52.00°W to 5.96°N, 57.02°W). ASC rarely falls below 1000 m and commonly exceeds 3–4000 m, with some peaks >7000 m. Unlike the other two sections, NSC continuously oscillates between stretches of net erosion and accretion. An erosional site is always found adjacent and to the east of an accretionary site, corresponding to each mudbank migrating westwards and causing erosion where it was originally located in 1988 and accretion where it was located in 2023. The largest ASC values were located at sites of mudbank migration and the headland B4, Coppename Nature Reserve, Suriname.

ASC rates dropped significantly between the second and the third sections, which spans the country of Guyana (5.96°N, 57.02°W to 7.68°N, 58.80°W) (ANOVA test of significant difference, F-statistic = 1931, p-value = 0.001; Figure 5). More than 86% of transects in this section had ASC values < 1500 m. Negative NSC values persisted along the majority of this coastline, particularly between the Suriname-Guyana border and the Demerara River. There were notable exceptions at the major settlements of Waterloo (D1), Georgetown (D2) and Anna Regina (D3) where shoreline position remained relatively static between 1988 and 2016, followed by more recent rapid shoreline accretion.

3.2 | Speed and nature of mudbank migration

Mudbanks initially weld to the coastline at site A0 situated east of Cayenne, French Guiana (Figure 1). Mangrove extent at A0 reduced

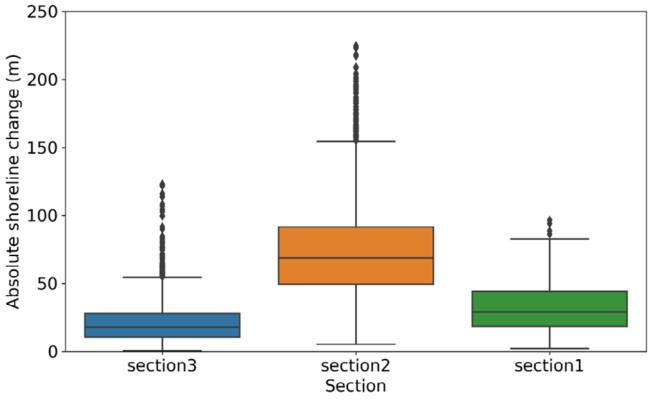

FIGURE 5 Boxplot of distribution of ASC values for every transect in Section 1: Amapá, northern Brazil, Section 2: mudbank section, and Section 3: Guyana. There was a statistically significantly larger mean ASC value in Section 2, that contains the migrating mudbanks, than in Sections 1 and 3.

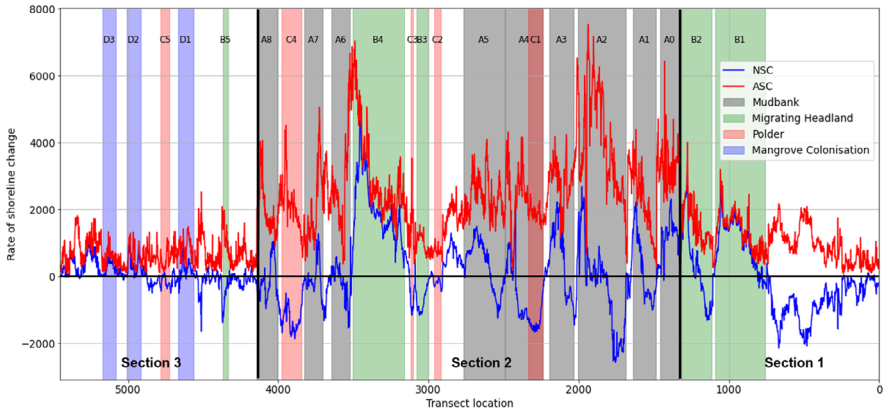

FIGURE 4 ASC (red) and NSC (blue) between 1988 and 2023 across the Guiana coastline. For NSC positive (negative) values correspond to net accretion (erosion). The shoreline is classified into a series of shoreline types; the areas in white are predominantly river outlets or other sections of coastline that separate the coastal landforms. The locations of different coastal landforms are identified in Figure 1, and a satellite image of each is provided in Figure 3. The sea wall in Section 3 is demarcated by a horizontal black line. The three sections, displaying distinct patterns in NSC and ASC values, are highlighted.

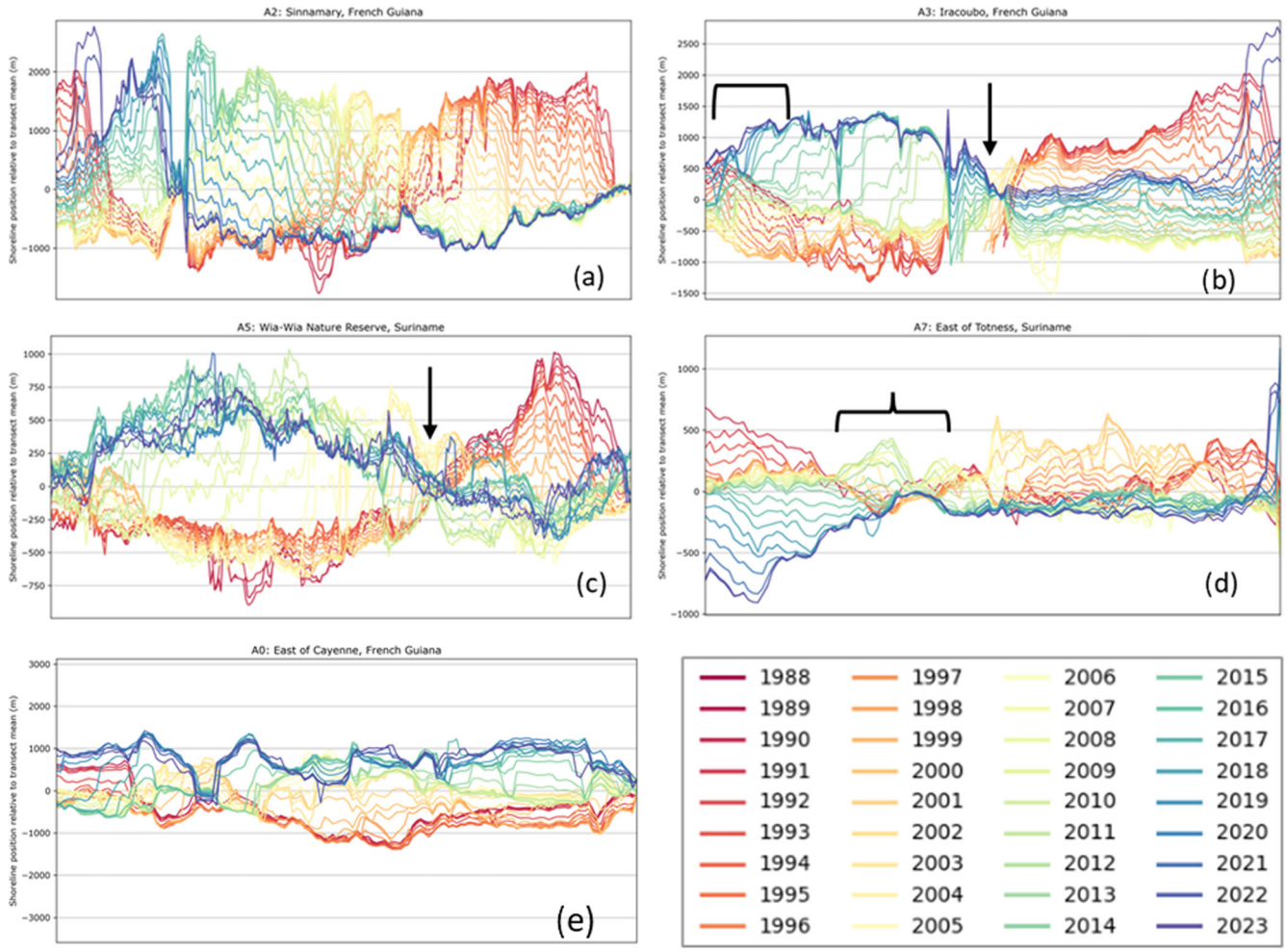

FIGURE 6 Change in the profile of maximum mangrove extent for five of the mudbanks identified across the Guiana coastline. The darkest red line corresponds to shoreline position in 1988 and darkest blue to 2023. The vertical black arrows in (b) and (c) denote the pivot points where ASC values remain low as the mudbanks abruptly migrated over this section of coastline. Square brackets in (b) highlights the leading edge of mudbank A3 migrating over the polder at Mana. The curly brackets in (d) denotes the extent of mudbank A7, Totness in 2010, prior to its migration over the polder. The profiles of all mudbanks can be found in Appendix S3.

between 1988 and 1993 as the mudbank initially present at this site migrated alongshore. The mudbank present at A0 in 2023 was formed during two abrupt phases of mangrove colonisation: 1997–2002 and 2012–2019, with mangrove extent remaining relatively constant in the intervening period. Since 2021, the trailing edge of mudbank A0 has eroded, suggesting that it is beginning its north-westerly migration (Figure 6e).

The other eight active, migratory mudbanks identified across the Guiana coastline were heterogeneous in terms of (i) rate of alongshore migration, (ii) rates of NSC and ASC and (iii) whether migration was continuous or abrupt (Table 2).

The mudbanks situated closer to the Amazon delta migrated alongshore at the fastest rates (Table 2). Mudbank A2, Sinnamary, was the fastest moving mudbank, with its leading edge migrating 47.2 km in 34 years, equating to a mean rate of 1.38 km year^{-1}. In comparison, the adjacent mudbanks, A1, Macouria, and A3, Iracouba, migrated alongshore 24.5 and 21.7 km, respectively, in the same time period (Figures 1 and 4 and Appendix S1).

Mudbanks exhibit either a graded or abrupt form of alongshore migration. Graded migration consists of consistent erosion (progradation) on an annual basis to the lee (leading) side of the mudbank (Figure 6a,d). In comparison, the leading edge of a mudbank exhibiting an abrupt migration style remains relatively static for many years while its trailing edge continuously erodes; this is followed by a relatively short period when mangrove rapidly establishes at an adjacent downdrift location. These abruptly migrating mudbanks have a pivot point, where ASC rates were very low compared to adjacent areas (see arrows, Figure 6b,c). The abrupt colonisation of mangroves downdrift of these pivot points occurred between 2006–2009, 2005–2008 and 2016–2018 at sites A3, Sinnamary A5, Wia-Wia, and A8, Totness, respectively. This abrupt migration style can alter the profile of the mudbank. For example, mudbank A5, Wia-Wia, Suriname, had a relatively narrow alongshore and wide cross-shore profile in 1988, whereas in 2023, it had a broader alongshore and narrower cross-shore profile (Figure 6c).

Mudbanks A0–A5 are situated close (< 50 km) to each other and the position of each of these mudbanks in 2023 overlapped with the position of the preceding mudbank in 1988 (Appendix S1). A gap spanning > 180 km exists between mudbank A5, Wia-Wia, Suriname, and A6, Jenny, Suriname. This intermudbank region contains the Wia-Wia and Coppename Nature Reserve, and with the exception of polders C2 and C3 at Mataica Beach and Paramaribo, the coastline lacks significant

TABLE 2 Amount of alongshore migration at the leading and trailing edge of each mudbank between 1988 and 2023, along with categorisation of the migration type for eight of the mudbanks identified along the Guiana coastline (for locations see Figure 1).

Mudbank	Leading edge migration distance (km)	Trailing edge migration distance (km)	Abrupt or graded migration
A1, Macouria, French Guiana	24.5	21.2	Graded
A2, Sinnamary, French Guiana	47.2	47.8	Graded
A3, Iracoubo, French Guiana	21.7	25.7	Abrupt
A4, Mana, French Guiana	26.9	27.6	Graded
A5, Wia-Wia Nature Reserve, Suriname	35.8	19.3	Abrupt
A6, Jenny, Suriname	15.7	13.9	Graded
A7, East Totness, Suriname	19.1	17.9	Graded
A8, Totness, Suriname	8.9	30.3	Abrupt

Note: A0, Cayenne, is omitted because it had not formed in 1988. Graphical representation of this information is contained in Appendix S5.

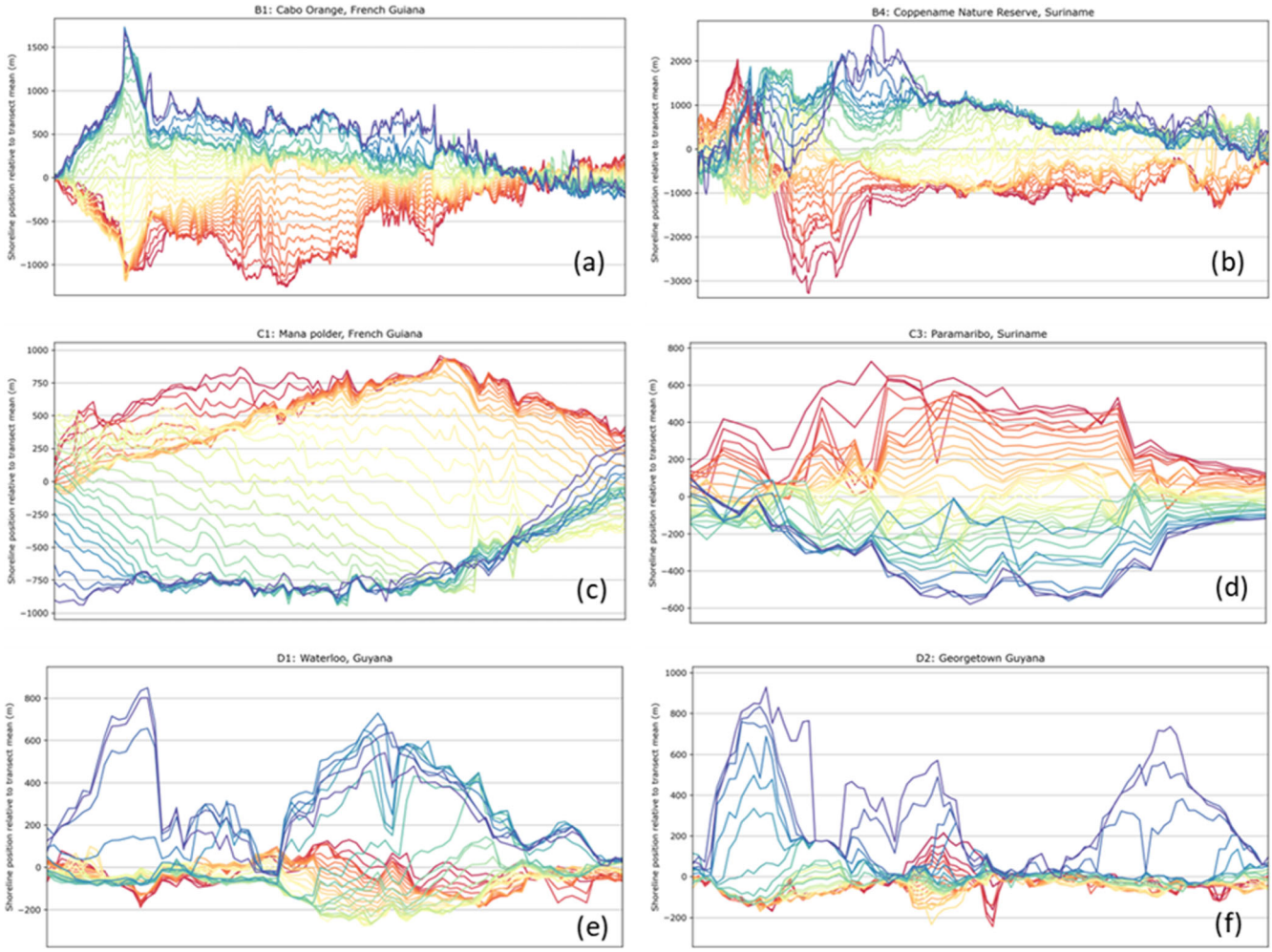

FIGURE 7 Relative shoreline position plots for the other landforms identified along the Guiana coastline: (a, b) realigning headlands, (c, d) polder regions and (e, f) regions of pronounced shoreline accretion influence by human modification. See Figure 6 caption for a description of the colour ramp. The relative positions of the landforms are shown in Figure 1, and their profiles can be found in Appendix S3.

human intervention. The Coppename Nature Reserve, B4, exhibited exceptional rates of shoreline accretion, particularly between 2002–2004, 2007–2008 and 2011–2012, when positive NSC rates > 400 m year^{-1} were recorded along some transects, greater than the rates shown by many of the mudbanks (Figure 7b). However, this shoreline has continuously accreted rather than exhibiting the erosion–accretion pattern typical of mudbank dynamics.

The response of mudbanks as they migrate past the site of shoreline polders differs. The shoreline at polder C4, Totness, Suriname, has retreated every year since 1988 (Figure 7c), whereas mangrove colonisation and shoreline progradation have occurred since 2021 at polder C1, Mana, Suriname (Figure 7c).

The shoreline position at D sites remained relatively stable until 2016 at Anna Regina and 2020 at Waterloo and Georgetown. This

was succeeded by a period of rapid shoreline accretion, measuring up to 720, 430 and 452 m year^{-1} at Waterloo, Georgetown and Anna Regina, respectively (Figure 7e,f). Shorelines stabilised after 2–3 years of rapid accretion, with most transects exhibiting < 100 m of ASC between 2022 and 2023.

3.3 | Rates of shoreline change and their teleconnections to wave climate and major climatological indices

The mean significant wave height across the Guiana coastline during the study period 1988–2023 was 1.28 m, and the extreme wave height, defined here as the 95th percentile of significant wave heights, was 2.03 m (Figure 8a). The extreme wave height increased from an average of 2.02 m between 1988 and 1993 to 2.08 m between 2018 and 2023, with the largest extreme wave heights recorded in 2017 (2.13 m) (Figure 8c). The number of days between 1988 and 2023 with extreme significant wave heights above 2.03 m was lower in Section 3 (Guyana) than the other two sections (Figure 8b). Mean sea levels consistently increased between 1988 and 2023 (Figure 8d). When superimposing the 18.6-year nodal cycle on MHW levels, there was a reduction in water levels between 2006 and 2011 before they began to increase, at a faster rate, after 2012 (as seen later in Figure 10e).

Between 1988 and 1998, the pan-Guiana coastline underwent net erosion, followed by a period of near-zero NSC or net accretion between 1999 and 2014, before returning to net erosion between 2014 and 2023 (Figure 9a). While there was no increasing or decreasing trend in erosion or accretion across Guiana during the study period, there was a statistically significant increasing trend in ASC ($r = 18.93$, p-value $= 0.001$; Figure 9b). ASC across Guiana was most strongly correlated with mean sea level ($r = 0.57$), with an increase in ASC as mean sea level increased (Figure 10e). NSC across Guiana had the strongest correlation with the 18.6-year nodal cycle ($r = 0.48$) (Figure 9a,f). There were only weak to moderate correlations with all other external forcing factors at a pan-Guiana scale. The site with the strongest statistical relationship with the 18.6-year nodal cycle was A0, Cayenne, where two distinct periods of mudbank correlation coincided with high MHW ($r = 0.63$, Figure 10g).

The spike in ASC values in 2007 corresponded to the simultaneous spikes in ASC values for mudbanks A2, A5 and A6 (Figure 10a–c) as well as the polder at Mana (C1). There were also less significant increases in ASC values in 2007 at mudbanks A4, Mana A7, East Totness, and A8, Totness (Appendix S4). At all of these sites, ASC values were lower between (i) 2005 and 2006 and (ii) 2008 and 2010. This signal aligns with a major positive NAO year in 2007, preceded and followed by low or negative NAO index values (Figure 10a–c). The largest ASC values recorded at mudbanks A3, Iracoubo, and A5, Wia-Wia, and the migrating headland at B4, Coppename, coincided with the subsequent major positive NAO year of 2012. However, no site recorded large ASC during both 2007 and 2012. The relationship between NAO and ASC was weaker for the rest of the time period,

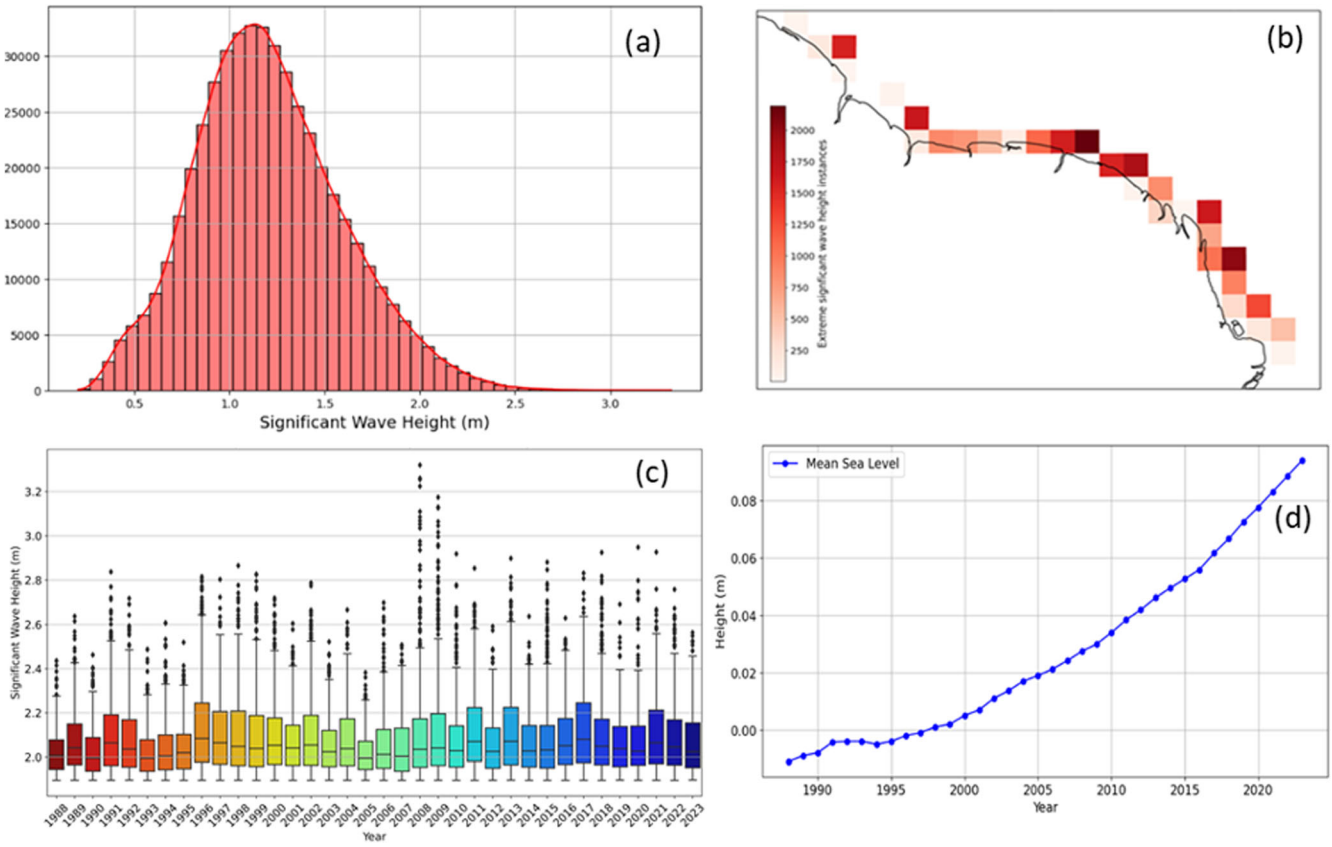

FIGURE 8 Changes in wave and sea level conditions across space and time. (a) Distribution of significant wave height across the Guiana coastline 1988–2023; (b) count per pixel of number of days with extreme waves, defined here as the 95th percentile of significant wave height; (c) distribution of extreme waves per year; (d) mean annual sea level across Guiana 1988–2023. All data were derived from ERA5 reanalysis products (Table 1; ECMWF, 2014).

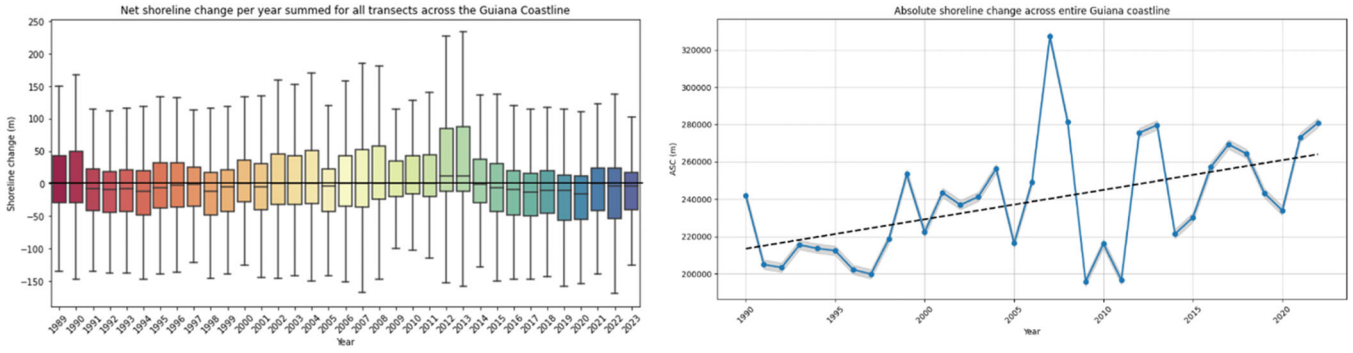

FIGURE 9 (a) Boxplot of NSC across all transects along the Guiana coastline 1988–2023. Positive (negative) values corresponding to net accretion (erosion). (b) Total magnitude of shoreline change summed over every transect each year. Between 1988 and 2023, there was no trend in NSC, but there was an increasing trend in ASC. The regression line in black shows an average increase in ASC of 1893 m per year and uncertainty is shown in grey.

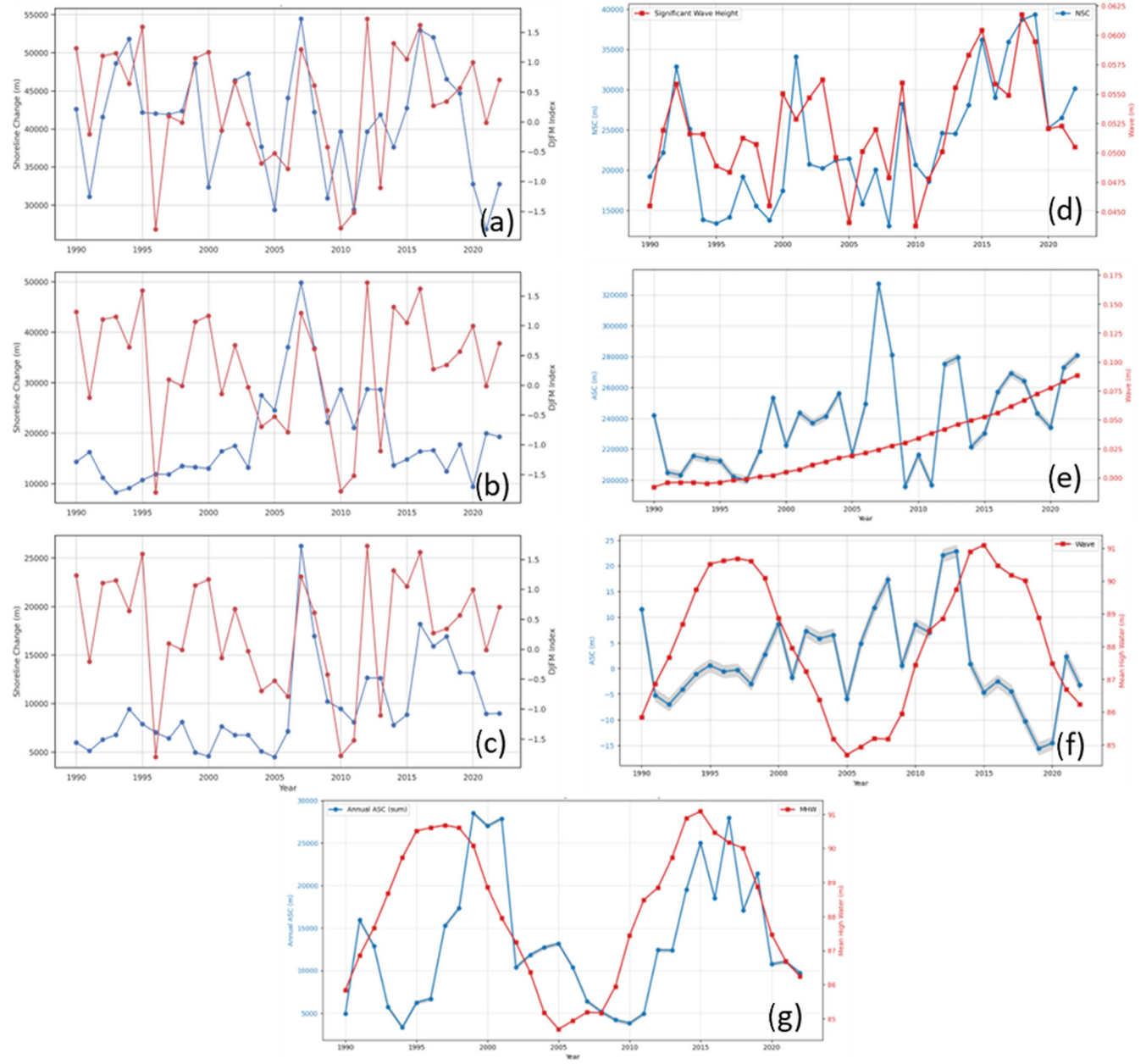

FIGURE 10 (a)–(c) Simultaneous peaks in ASC values in 2007 overlaid with the North Atlantic oscillation ONDJFM at (a) mudbank A2, Sinnamary, French Guiana; (b) mudbank A5, Wia-Wia nature reserve, Suriname; (c) mudbank A6, Jenny, Suriname; (d) NSC and significant wave height at Section 1, Uaça, Brazil; (e) pan-Guiana ASC and mean sea level; (f) pan-Guiana NSC and 18.6 year cycle of mean high water level; (g) ASC at mudbank A0, Cayenne, and 18.6-year cycle of mean high water level. Uncertainty is shown by the transparent grey bars. For site-based locations, uncertainty was smaller than the width of the blue line.

and only weak to moderate correlations between NAO and ASC were recorded during the entire study period, both at a site level and at the pan-Guiana level (Appendix S4).

Section 1 (Amapá, northern Brazil) was the only section that exhibited a statistically significant strong positive correlation between ASC and significant wave height ($r = 0.7$; Figure 10d). Other individual sites, including mudbanks A2, Sinnamary, ($r = 0.62$) and A6, Jenny, Suriname ($r = 0.58$), and migrating headland B2, Pointe Béhague ($r = 0.60$), exhibited moderate to strong correlations between the alongshore component of significant wave height, C_L and ASC. However, by contrast, there was no statistically significant relationship between wave and shoreline change metrics in Sections 2 and 3 or along the Guiana coastline as a whole. The sites that had the strongest correlations with mean sea level were mudbanks A3, Iracoubo, ($r = 0.84$) and A4, Mana, ($r = 0.81$) and the Mataica polder ($r = 0.76$). All shoreline change values had weak to moderate correlations with the ENSO metrics.

4 | DISCUSSION

This paper has generated the first ever pan-Guiana dataset of annual rates of shoreline change over a 35-year period (1988–2023). The Guiana coastline has previously benefited from extensive research at a landform (Fromard et al., 2004), national (de Jong et al., 2021) and Pan-Guiana scale (Augustinus, 2004), but no detailed annual analysis of the entire region has been conducted at this temporal scale. Using the seaward extent of mangrove forest as the shoreline proxy, this analysis has identified new information about the dynamics of the Guiana coastline: (i) there are nine sites (A0–A8) that exhibit a cycle of mangrove colonisation and erosion caused by bank–interbank phases of alongshore mudbank migration (Figure 1); (ii) each of these nine sites exhibits a different speed and form of alongshore migration; (iii) there is no consistent periodicity in bank–interbank phases, but the time difference between mudbanks is a minimum of 40 years compared with the previously commonly accepted period of 30 years (Anthony et al., 2010; Anthony et al., 2014; Fromard et al., 2004); (iv) these nine sites are located along just two distinct stretches of Guiana coastline, with no evidence of coastline oscillations along the majority of the Suriname and entire Guyana coastlines; and (v) at these other sites, other coastal landforms, including migrating headlands and sites of anthropogenic modification dominate shoreline change processes. Correlation analysis between shoreline change metrics and external forcing factors revealed few statistically significant relationships. However, changes in mean sea level and the 18.6-year lunar cycle have the largest impact on the Guiana coastline as a whole, whereas wave metrics have a greater impact at a site scale.

The alongshore migration rates of the nine mudbanks between 1988 and 2023 varied between 0.26 and 1.38 km year^{-1}, notably slower than the previously suggested average rate of 0.9–5 km year^{-1} (Abascal-Zorrilla et al., 2024; Augustinus, 2004; Froidefond et al., 1988; Gardel & Gratiot, 2005). The disparities in migration rates between individual mudbanks confirm that there is no standard periodicity in mudbank formation and can be partially attributed to differences in dominant shoreline direction. The mudbanks that have migrated at the fastest rate, A1–A4, are situated on coastlines in French Guiana that primarily run northwest to southeast, whereas the mudbanks A6–A8, which have migrated at a slower rate, are located on north-facing coastlines in West Suriname. This results from the typical incidence angle of the highest energy waves (that tend to come from an east-northeast direction) being greater at sites A1–A4 than A6–A8, which has been shown to increase mud mobilisation and alongshore migration rates (Gratiot et al., 2007). However, the mudbank A2, Sinnamary has migrated at more than double the speed of the two adjacent mudbanks, even though the dominant shoreline direction at the three sites is very similar (Table 2). There must, therefore, be other factors that affect alongshore migration. These are likely to include local differences in bathymetry, sediment rheology and nearshore hydrodynamics (waves and currents).

4.1 | Going beyond oscillatory mudbank dynamics

Characterisation of the Guiana coastline has previously focussed on the model of approximately 20–25 shore-attached mudbanks forming a continuous oscillatory signal of mangrove colonisation and accretion (Anthony et al., 2014; Eisma et al., 1991). However, the identification of just nine mudbanks along only two distinct subsections of the Guiana coastline supports an alternative model that, rather than being shore-attached, mudbanks remain as features disconnected from the coastline, and fluid-mud suspension is advected towards the coastline during high wave events (Allison & Lee, 2004; Orseau et al., 2020).

Furthermore, it is clear that there are important interactions between migratory mudbanks and the river systems that discharge onto the Guiana coast. Such dynamics can trigger a break in the usual bank—interbank, mud migration—mangrove colonisation dichotomy. Under such conditions, the discontinuity in mudbank migration can make consolidation processes take longer and thus contribute to a temporary slowing of mangrove colonisation (Gardel et al., 2011). Gardel et al. (2022) provide a remote sensing-based classification of river types along the shoreline. Three basic types are identified: (1) river mouths diverted westward by capes and spits built from multidecadal to multi-millennial accumulation of the westward mud conveyor, some (closer to the Amazon) constrained by bedrock outcrops (Type 1a) and some unconstrained (Type 1b); (2) small river mouths in French Guiana fixed around bedrock headlands; and (3) large river mouths characterised by high water discharge that imparts an orientation normal to the coast; the largest two belong to this type (the Essequibo in Guyana and the Maroni on the border between French Guiana and Suriname). In Type 2 setting, Orseau et al. (2017) and, through modelling, Abascal-Zorrilla et al. (2024) document marine-estuarine interactions in the Madury estuary, French Guiana. Between 2012 and 2018, a mudbank migrated across the mouth of the Madury River. During the rainy season, the strength of river flow limited mud deposition in the navigation channel and at the mouth of the estuary; rather, mud deposition occurred on the sandy beaches that flank the outer estuary and on the front edge of the mudbank. By contrast, during the dry season with low river discharge, fluid mud was deposited in the navigation channel of the estuary and at the river mouth, leading to an increase in intertidal areas, particularly on the eastern side of the estuary. This pattern suggests that river discharge affects the coastal current in a way akin to a hydraulic groyne effect (Orseau et al., 2020). This hydraulic groyne effect is proposed to be the cause of the abrupt nature of migration observed at mudbanks A2 (Iracoubo, French Guiana) (Figure 6b) and A5

(Wia-Wia Nature Reserve, Suriname) (Figure 6c); however, no river mouth was identified adjacent to mudbank A8, Totness, Suriname (Appendix S1), suggesting other factors, such as anthropogenic modification to the coastline, may disrupt any individual mudbank's continuous alongshore migration.

Rather more dramatically, Type 1b settings are characterised by lower river discharges and lower tidal ranges than Type 1a river mouths and thus display considerable, long-term downdrift mudcape extensions and deflections of the river outlet. A particular example is the mudcape of Pointe Isere, French Guiana, which has diverted the Mana River westwards since at least the nineteenth century (Plaziat & Augustinus, 2004). Using a > 60-year record of aerial photographs and satellite images, Jolivet et al. (2019) document massive retreat of the Isere shoreline (>1 km between 1955 and 1972) and spit elongation, finally resulting, in 2001, in a breach that created a new direct outlet for the Mana River several kilometres to the east of its former location (it seems likely that there will be a new cycle of mudcape formation and its westerly extension at the mouth of the new Mana River). In 2011, a gradual onshore welding of a large mudbank then sealed the ancestral mouth of the Mana. Interestingly, Jolivet et al. (2019) note that during the continuous erosion of Pointe Isère, the longshore passage of several mud banks did not mitigate the rates of erosion, suggesting 'the need to go beyond the common vision of such change in terms of mud-bank (shoreline accretion) and inter-bank (shoreline erosion) phases that cover timescales of the order of years to a decade.' (Jolivet et al., 2019, 185). Our analysis supports these views, as the pattern of change at the Mana River is gradual, not abrupt (Table 2 and Appendix S1).

The statistically significant reduction in ASC rates along the Guyana coastline (Figure 4) and lack of oscillatory signal in mangrove extent has been attributed to the presence of a sea wall running between the Suriname-Guyana border and Georgetown (Deltares, 2020; Vaughn, 2018). This wall prevents mudbanks from welding to this coastline, increases mud-bank liquefaction, and encloses mangrove forest (Anthony & Gratiot, 2012). There is still sufficient sediment in the water column for shore-attached mudbanks to form because exceptional rates of accretion exceeding 430 m year^{-1} have occurred where anthropogenic structures have been installed orthogonal to the dominant shoreline direction (D1-D3) (Figure 7e,f). Ahmad & Lakhan (2012) identified a 30-year oscillation in shoreline position that was still present between 1947 and 1987, but the analysis reported here shows that since this time, the Guyana coastline has not exhibited these mudbank-driven patterns of coastal change.

Even along the French Guiana and Suriname coastlines, the dominant oscillatory pattern is reduced by the presence of emplaced polders. The location-specific signal is dependent upon local factors, with more of an oscillatory pattern remaining in the presence of larger migratory mudbanks such as A3, Mana, French Guiana (Figure 7c) than by smaller mudbanks including mudbank A7, Totness, Suriname, where the oscillation signal has stopped completely (Figure 6d).

4.2 | Linking shoreline change dynamics to external forcing factors

The transition from net erosion to net accretion at the turn of the last century has previously been documented (Gratiot et al., 2008; Walcker et al., 2015); however, the return of the system to a period of net loss after 2012 has not previously been reported. Further, NSC was closer to zero between 2022 and 2023 compared to the preceding 4 years, suggesting that the system is returning to another phase of near-zero or positive NSC values (Figures 9a and 10f).

While the Guiana shoreline has become more dynamic over time as mean sea levels have increased on average by 0.003 m year^{-1} (Figure 8d), there has been no overall net loss or gain of mangrove extent within the system. This aligns with previous suggestions that mean sea level does not appear to be driving net mangrove retreat in this region (Walcker et al., 2015). However, there was a statistically significant negative correlation between NSC in Section 1 and both mean sea level and H_s, meaning erosion rates increased here as sea levels and significant wave heights increased (Figure 10d). The different signals between Sections 1 and 2 can be attributed to the diminished sediment supply and lack of shore-welded mudbanks in Section 1 (Froidefond et al., 1988), whereas the mudbanks in Section 2 mitigate the increased erosional power of stronger waves and higher mean sea levels. These findings echo some of the criticisms of global shoreline change studies which predict the disappearance of sandy beaches under sea level rise (e.g., Vousdoukas et al., 2020) which point to the importance of sediment supply in allowing the persistence, or even progradation, of shorelines in the presence of a positive sediment budget (Cooper et al., 2020). Future research, however, does need to determine whether a threshold mean sea level exists at which point the higher water levels overwhelm the mitigating effect of the huge sediment supply to Section 2. In a mangrove ecosystem context, a threshold of 7 mm year^{-1} sea level rise for wetland persistence has been proposed based on paleo-ecological evidence (Saintilan et al., 2020) but will most likely be subject to regional variation with different environmental settings.

4.3 | The evolution of the Guiana coastline up to 2040

It is clear from this analysis that the future evolution of the Guiana coastline will be different between the three sections (Figure 4). Section 1, Amapá, northern Brazil, is the section most susceptible to increases in mean sea level and extreme waves, attributed to the limited sediment supply to this coastline compared to the mudbanks of Section 2. It is hypothesised that rates of erosion will continue to increase across Section 1. The differences in the characteristics of the mudbanks and other landforms within Section 2 mean that there is likely to be no single signal in the change of this coastline over the next two decades. By extrapolating the nodal cycle signal, it is predicted that mangrove extent will remain stable or increase for the next 8–10 years, as the 18.6-year nodal cycle reduces sea levels or tapers the rate of sea level rise. However, it is expected that larger rates of erosion will be experienced from approximately 2030 when the 18.6-year nodal cycle moves into another positive phase. Future research should focus on the differing rates of shoreline change caused by the passage of mudbanks past polders in Section 2. For Section 3, Guyana, there is clear evidence that the human interventions at sites D1–3 have successfully encouraged mangrove expansion. As elsewhere (e.g., Mekong Delta, Phan et al., 2022; Sundarbans, Rahman et al., 2025), it is anthropogenic coastal management

decisions, rather than oceanic or climatological external forcing factors, that will play the biggest role in determining the magnitude and direction of shoreline change in Guyana over the next two decades.

5 | CONCLUSION

The application of shoreline change analysis to 535 Landsat scenes for the period 1988–2023 has produced a record of mangrove forest seaward margin change along the entire 1500 km of the coastline of the Guineas, from the northern margins of the Amazon delta to the southern limit of the R. Orinoco. Sampling at an alongshore interval of 200 m generated 5644 shore-normal transects; with 36 entries, the resulting database contains over 200 000 datapoints. The consistency of application of this methodology makes possible a coherent multiscale analysis of shoreline dynamics. Correlation analysis was used to determine the statistical relationships between multiple external forcing factors and shoreline change metrics from an individual mudbank to the pan-Guiana level. Metrics with low temporal frequencies, such as the 18.6-year nodal tidal cycle, have the greatest control at the pan-Guiana shoreline change scale, whereas short-term wave metrics are more important for understanding changes in shoreline condition at the local scale.

In temporal terms, the shoreline as a whole did not experience significant net loss or accretion between 1988 and 2023 but rather went through shorter phases of net accretion or erosion. Between 1988 and 1998, the Guiana shoreline exhibited net erosion or near-zero shoreline change values. This was succeeded by a period of net accretion between 1998 and 2012, before a dramatic shift back to net erosion 2012–2021. Since 2021, NSC values have returned closer to zero, indicating an impending shift back to a period of shoreline advancement across the Guianas. In the assessment of seven potential forcing factors for explaining the pattern of change, no clear controlling factors were identified, although the shifts in phase from net erosion to accretion coincided with increasing and decreasing phases in the 18.6 nodal tide cycle.

In spatial terms, the shoreline can be divided into three distinct sections. Section 1, the Amazon delta to the site where mudbanks first weld to the coastline in French Guiana, has an easterly facing coastline and is characterised by consistent shoreline retreat. There is some evidence that erosion rates have increased in this section with sea level rise and increases in significant wave heights over the whole study period. In Section 2, the region which contains migratory mudbanks in French Guiana and Suriname, this analysis has shown that, and unlike the conclusions of some earlier studies, the dynamics of the Guinea coastline cannot be explained by a simple oscillatory behaviour relating to the presence or absence of mudbanks; along many parts of the coast, the interaction between alongshore mudbank migration and river/estuary hydrodynamics has generated complex patterns of coastal change. Where erosion/deposition shifts are seen over time, this analysis has shown that alongshore mudbank migration rate has been significantly slower than previously reported rates; thus, where an oscillatory signal is present, it is at a time course longer than the frequently quoted duration of 30 years. In addition, the large-scale alongshore record includes near-natural coastal sections which show no oscillatory behaviour. In Section 3, which consists of the entire coastline of the country of Guyana, the shoreline change record is dominated by the influence of a continuous shore-parallel seawall. This structure is the most pervasive of a series of anthropogenic interventions which influence shoreline dynamics; others include shore-normal groynes and jetties and constructed polders.

Future large-scale analysis of shoreline change using this dataset and others is essential for understanding the dominant processes controlling the complex space–time dynamics of this coastline. *In situ* measurements remain necessary for understanding local scale processes and subtidal dynamics that cannot be captured by larger scale satellite imagery.

ACKNOWLEDGEMENTS

Initial stages of this research were undertaken as part of the UKRI NERC/ESRC Data, Risk and Environmental Analytical Methods (DREAM) Centre for Doctoral Training, grant/award numbers: NE/M009009/1, NE/R011265/1. The authors would like to thank Dr. Mike Bithell, University of Cambridge, for his contribution towards developing research objectives and Professor Phil Woodworth, National Oceanographic Centre, for obtaining and analysing the tidal data used in this project.

CONFLICT OF INTEREST STATEMENT

There are no potential conflicts of interest.

DATA AVAILABILITY STATEMENT

The data that support the findings of this study are openly available in Pan-Guiana shoreline position 1988 - 2023 at https://zenodo.org/records/15191879, reference number 10.5281/zenodo.15191879.

PERMISSION TO REPRODUCE MATERIAL FROM OTHER SOURCES

This manuscript uses image data from the Landsat and Planet satellite platforms. All image data is open-sourced and available for public use.

REFERENCES

Abascal-Zorrilla, N., Huybrechts, N., Orseau, S., Vantrepotte, V., Anthony, E. & Gardel, A. (2024) Numerical investigation of the sediment load exchange between a coastal mud bank and its neighbouring estuary. *Water*, 16(20), 2885. Available from: https://doi.org/10.3390/w16202885

Ahmad, S.R. & Lakhan, V.C. (2012) GIS-based analysis and modeling of coastline advance and retreat along the coast of Guyana. *Marine Geodesy*, 35(1), 1–15. Available from: https://doi.org/10.1080/01490419.2011.637851

Allison, M.A., Lee, M.T., Ogston, A.S. & Aller, R.C. (2000) Origin of Amazon mudbanks along the northeastern coast of South America. *Marine Geology*, 163(1-4), 241–256. Available from: https://doi.org/10.1016/S0025-3227(99)00120-6

Allison, M.A. & Lee, M.T. (2004) Sediment exchange between Amazon mudbanks and shore-fringing mangroves in French Guiana. *Marine Geology*, 208(2-4), 169–190. Available from: https://doi.org/10.1016/j.margeo.2004.04.026

Anthony, E.J., Gardel, A. & Gratiot, N. (2014) Fluvial sediment supply, mud banks, cheniers and the morphodynamics of the coast of South America between the Amazon and Orinoco river mouths. *Geological Society, London, Special Publications*, 388(1), 533–560. Available from: https://doi.org/10.1144/SP388.8

Anthony, E.J., Gardel, A., Gratiot, N., Proisy, C., Allison, M.A., Dolique, F., et al. (2010) The Amazon-influenced muddy coast of South America: a review of mud-bank–shoreline interactions. *Earth-Science Reviews*, 103(3), 99–121. Available from: https://doi.org/10.1016/j.earscirev.2010.09.008

Anthony, E.J. & Gratiot, N. (2012) Coastal engineering and large-scale mangrove destruction in Guyana, South America: averting an

environmental catastrophe in the making. *Ecological Engineering*, 47, 268–273. Available from: https://doi.org/10.1016/j.ecoleng.2012.07.005

Augustinus, P.G.E.F. (2004) The influence of the trade winds on the coastal development of the Guianas at various scale levels: a synthesis. Marine geology, material exchange between the upper continental shelf and mangrove fringed coasts with special reference to the N. *Amazon-Guianas Coast*, 208, 145–151. Available from: https://doi.org/10.1016/j.margeo.2004.04.007

Best, Ü.S.N., van der Wegen, M., Dijkstra, J., Reyns, J., van Prooijen, B.C. & Roelvink, D. (2022) Wave attenuation potential, sediment properties and mangrove growth dynamics data over Guyana's intertidal mudflats: assessing the potential of mangrove restoration works. *Earth System Scientific Data*, 14, 2445–2462. Available from: https://doi.org/10.5194/essd-14-2445-2022

Best, Ü.S.N., Legay, A., Reyns, J. & van der Wegen, M. (2025) Morphodynamic adaptation timescales of the Guyana mangrove-mudflat system: are coastlines shaped by migrating mudbanks more resilient against sea level rise? *Earth Surface Processes and Landforms*, 50(10), e70135. Available from: https://doi.org/10.1002/esp.70135

Boak, E.H. & Turner, I.L. (2005) Shoreline definition and detection: a review. *Journal of Coastal Research*, 21(4), 688–703. Available from: https://doi.org/10.2112/03-0071.1

Brunier, G., Anthony, E.J., Gratiot, N. & Gardel, A. (2019) Exceptional rates and mechanisms of muddy shoreline retreat following mangrove removal. *Earth Surface Processes and Landforms*, 44(8), 1559–1571. Available from: https://doi.org/10.1002/esp.4593

Cooper, J.A.G., Masselink, G. & Coco, G. (2020) Sandy beaches can survive sea-level rise. *Nature Climate Change*, 10, 993–995. Available from: https://doi.org/10.1038/s41558-020-00934-2

de Jong, S.M., Shen, Y., de Vries, J., Bijnaar, G., van Maanen, B., Augustinus, P., et al. (2021) Mapping mangrove dynamics and colonization patterns at the Suriname coast using historic satellite data and the LandTrendr algorithm. *International Journal of Applied Earth Observation and Geoinformation*, 97, 102293. Available from: https://doi.org/10.1016/j.jag.2020.102293

de Vries, J., van Maanen, B., Ruessink, G., Verweij, P.A. & de Jong, S.M. (2022) Multi-decadal coastline dynamics in Suriname controlled by migrating subtidal mudbanks. *Earth Surface Processes and Landforms*, 47(10), 2500–2517. Available from: https://doi.org/10.1002/esp.5390

Deltares. (2020) Guyana: mangrove engineering guidance. Retrieved November 1, 2024. https://publications.deltares.nl/11207078.pdf

Dytham, C. (2011) *Choosing and using statistics: a biologist's guide*. Chichester, West Sussex: John Wiley & Sons.

ECMWF, S.P. (2014) In IFS documentation CY40R1 part IV: physical processes. ECMWF: Reading, UK, pp.111–113.

Eisma, D., Augustinus, P.G.E.F. & Alexander, C. (1991) Recent and subrecent changes in the dispersal of Amazon mud. *Netherlands Journal of Sea Research*, 28(3), 181–192. Available from: https://doi.org/10.1016/0077-7579(91)90016-T

Ellison, J.C. (2009) Geomorphology and sedimentology of mangroves. In: Perillo, G.M.E., Wolanski, E., Cahoon, D.R. & Brinson, M.M. (Eds.) *Coastal wetlands: an integrated ecosystem approach*. Amsterdam: Elsevier, pp. 565–591.

Fiot, J. & Gratiot, N. (2006) Structural effects of tidal exposures on mudflats along the French Guiana coast. *Marine Geology*, 228(1–4), 25–37. Available from: https://doi.org/10.1016/j.margeo.2005.12.009

Fox-Kemper, B., Hewitt, H.T., Xiao, C., Aðalgeirsdóttir, G. & Drijfhout, S.S. 2021. Ocean, cryosphere and sea level change. In: Masson-Delmotte, V., Zhai, P., Pirani, A., Connors, S.L., and Péan, C. (Eds.) *Climate change 2021: the physical science basis. Contribution of Working Group I to the Sixth Assessment Report of the Intergovernmental Panel on Climate Change*. Cambridge, UK and New York, NY, USA: Cambridge University Press, 1211–1362. https://doi.org/10.1017/9781009157896.011

Friess, D.A. & McKee, M. (2021) The history of surface-elevation paradigms in mangrove biogeomorphology. In: Sidik, F. & Friess, D.A. (Eds.) *Dynamic sedimentary environments of mangrove coasts*. Amsterdam: Elsevier, pp. 179–198.

Froidefond, J.M., Pujos, M. & Andre, X. (1988) Migration of mud banks and changing coastline in French Guiana. *Marine Geology*, 84(1-2), 19–30. Available from: https://doi.org/10.1016/0025-3227(88)90122-3

Fromard, F., Vega, C. & Proisy, C. (2004) Half a century of dynamic coastal change affecting mangrove shorelines of French Guiana. A case study based on remote sensing data analyses and field surveys. Marine geology, material exchange between the upper continental shelf and mangrove fringed coasts with special reference to the N. *Amazon-Guianas Coast*, 208, 265–280. Available from: https://doi.org/10.1016/j.margeo.2004.04.018

Gardel, A., Anthony, E.J. & Santos, V.F. (2022) A remote sensing-based classification approach for river mouths of the Amazon-influenced Guianas coast. *Regional Environmental Change*, 22, 65. Available from: https://doi.org/10.1007/s10113-022-01913-3

Gardel, A., Gensac, E., Anthony, E.J., Lesourd, S., Loisel, H. & Marin, D. (2011) Wave-formed mud bars: their morphodynamics and role in opportunistic mangrove colonization. *Journal of Coastal Research*, 64(1), 384–387. https://www.jstor.org/stable/26482198

Gardel, A. & Gratiot, N. (2005) A satellite image–based method for estimating rates of mud bank migration, French Guiana, South America. *Journal of Coastal Research*, 21(4), 720–728. Available from: https://doi.org/10.2112/03-0100.1

Gardel, A. & Gratiot, N. (2006) Monitoring of coastal dynamics in French Guiana from 16 years SPOT satellite images. *Journal of Coastal Research*, 39(1), 1502–1505. https://www.jstor.org/stable/25743005

Gensac, E., Lesourd, S., Gardel, A., Anthony, E.J., Proisy, C. & Loisel, H. (2011) Short-term prediction of the evolution of mangrove surface areas: the example of the mud banks of Kourou and Sinnamary, French Guiana. *Journal of Coastal Research*, 64(1), 388–392. Available from: https://www.jstor.org/stable/26482199

Gorelick, N., Hancher, M., Dixon, M., Ilyushchenko, S., Thau, D. & Moore, R. (2017) Google earth engine: planetary-scale geospatial analysis for everyone. *Remote Sensing of Environment*, 202(1), 18–27. Available from: https://doi.org/10.1016/j.rse.2017.06.031

Gratiot, N., Anthony, E.J., Gardel, A., Gaucherel, C., Proisy, C. & Wells, J.T. (2008) Significant contribution of the 18.6 year tidal cycle to regional coastal changes. *Nature Geoscience*, 1(3), 169–172. Available from: https://doi.org/10.1038/ngeo127

Gratiot, N., Gardel, A. & Anthony, E.J. (2007) Trade-wind waves and mud dynamics on the French Guiana coast, South America: input from ERA-40 wave data and field investigations. *Marine Geology*, 236(1-2), 15–26. Available from: https://doi.org/10.1016/j.margeo.2006.09.013

Haigh, I.D., Marcos, M., Talke, S.A., Woodworth, P.L., Hunter, J.R., Hague, B.S., et al. (2023) GESLA version 3: a major update to the global higher-frequency sea-level dataset. *Geophysical Data Journal*, 10(3), 293–314. Available from: https://doi.org/10.1002/gdj3.174

Jolivet, M., Gardel, A. & Anthony, E.J. (2019) Multi-decadal changes on the mud-dominated coast of Western French Guiana: implications for mesoscale shoreline mobility, river-mouth deflection, and sediment sorting. *Journal of Coastal Research*, 88(sp1), 185. Available from: https://doi.org/10.2112/SI88-014.1

Komar, P.D. & Inman, D.L. (1970) Longshore sand transport on beaches. *Journal of Geophysical Research*, 75(30), 5914–5927. Available from: https://doi.org/10.1029/JC075i030p05914

Kriegler, F.J., Malila, W.A., Nalepka, R.F. & Richardson, W. (1969) Preprocessing transformations and their effects on multispectral recognition. *Proceedings of the Sixth International Symposium on Remote Sensing of Environment*, 6, 97–131.

Le, H.T., Tran, T.V., Gyeltshen, S., Nguyen, C.P., Tran, D.X., Luu, T.H., et al. (2020) Characterizing spatiotemporal patterns of mangrove forests in Can Gio biosphere reserve using Sentinel-2 imagery. *Applied Sciences*, 10(12), 4058. Available from: https://doi.org/10.3390/app10124058

Lefebvre, J.P., Dolique, F. & Gratiot, N. (2004) Geomorphic evolution of a coastal mudflat under oceanic influences: an example from the dynamic shoreline of French Guiana. *Marine Geology*, 208(2-4), 191–205. Available from: https://doi.org/10.1016/j.margeo.2004.04.008

Menéndez, P., Losada, I.J., Torres- Ortega, S., Narayan, S. & Beck, M.W. (2020) The global flood protection benefits of mangroves. *Scientific Reports*, 10, 1–11. Available from: https://doi.org/10.1038/s41598-020-61136-6

NOAA. (2024a) North Atlantic Oscillation. Retrieved August 01, 2024. https://www.ncei.noaa.gov/access/monitoring/nao/

NOAA. (2024b) Multivariate ENSO index version 2 (MEI.v2). Retrieved August 01, 2024. https://psl.noaa.gov/enso/mei/

Orseau, S., Abascal Zorrilla, N., Huybrechts, N., Lesourd, S. & Gardel, A. (2020) Decadal-scale morphological evolution of a muddy open coast. *Marine Geology*, 420, 106048. Available from: https://doi.org/10.1016/j.margeo.2019.106048

Orseau, S., Lesourd, S., Huybrechts, N. & Gardel, A. (2017) 2017. Hydro-sedimentary processes of a shallow tropical estuary under Amazon influence. The Mahury Estuary, French Guiana. *Estuary and Coastal Shelf Science.*, 189, 252–266. Available from: https://doi.org/10.1016/j.ecss.2017.01.011

Phan, M.H., Marcel, J.F. & Stive, J. (2022) Managing mangroves and coastal land cover in the Mekong Delta. *Ocean and Coastal Management*, 219, 106013. Available from: https://doi.org/10.1016/j.ocecoaman.2021.106013

Planet Labs. (2023) Planet application program interface: In space for life on Earth. Retrieved. https://api.planet.com

Plaziat, J.C. & Augustinus, P.G. (2004) Evolution of progradation/erosion along the French Guiana mangrove coast: a comparison of mapped shorelines since the 18th century with Holocene data. *Marine Geology*, 208(2-4), 127–143. Available from: https://doi.org/10.1016/j.margeo.2004.04.006

Proisy, C., Gratiot, N., Anthony, EJ., Gardel, A., Fromard, F. & Heuret, P. (2009) Mud bank colonization by opportunistic mangroves: a case study from French Guiana using lidar data, *Continental Shelf Research*, 29 (3), 632–641 doi: https://doi.org/10.1016/j.csr.2008.09.017

Proisy, C., Walcker, R., Blanchard, E., Gardel, A. & Anthony, E.J. (2021) Chapter 2 - Mangroves: a natural early-warning system of erosion on open muddy coasts in French Guiana. In: Sidik, F. & Friess, D.A. (Eds.) *Dynamic sedimentary environments of mangrove coasts*. London, UK: Elsevier, pp. 47–66.

Rahman, KS., Dana, NH., Rahman, M., Mondal, H., Chen, L. & Islam, M. (2025) Degradation of mangrove forests in the Sundarbans: an assessment based on perspectives of mangrove resource collectors using the DPSIR framework. *Trees, Forests and People* 19, 100769. https://doi.org/10.1016/j.tfp.2024.100769

Rogers, M.S.J., Bithell, M., Brooks, S.M. & Spencer, T. (2021) VEdge_Detector: automated coastal vegetation edge detection using a convolutional neural network. *International Journal of Remote Sensing*, 42(3), 4805–4835. Available from: https://doi.org/10.1080/01431161.2021.1897185

Rovai, A.S., Twilley, R.R., Castañeda- Moya, E., Riul, P., Cifuentes- Jara, M., Manrow- Villalobos, M., et al. (2018) Global controls on carbon storage in mangrove soils. *Nature Climate Change*, 8(6), 534–538. Available from: https://doi.org/10.1038/s41558-018-0162-5

Saintilan, N., Khan, N., Ashe, E., Kelleway, J., Rogers, K., Woodroffe, C.D., et al. (2020) Thresholds of mangrove survival under rapid sea level rise. *Science*, 368, 1118–1121. Available from: https://doi.org/10.1126/science.aba2656

Satyanarayana, B., Mohamad, K.A., Idris, I.F., Husain, M.L. & Dahdouh-Guebas, F. (2011) Assessment of mangrove vegetation based on remote sensing and ground-truth measurements at Tumpat, Kelantan Delta, East Coast of Peninsular Malaysia. *International Journal of Remote Sensing*, 32(6), 1635–1650. Available from: https://doi.org/10.1080/01431160903586781

Saunier, S. (2021) TN on quality assessment for PlanetScope (DOVE). Retrieved September 02, 2024. https://earth.esa.int/eogateway/documents/20142/1305226/EDAP-REP-007-TN-on-Quality-Assessment-for-PlanetScope-DOVE-v1.2.pdf

Seneviratne, S.I., Zhang, X., Adnan, M., Badi, W. & Dereczynski, C. (2021) Weather and climate extreme events in a changing climate. In: Masson-Delmotte, V., Zhai, P., Pirani, A., Connors, S.L. & Péan, C. (Eds.) *Climate change 2021: the physical science basis*. Contribution of Working Group I to the Sixth Assessment Report of the Intergovernmental Panel on Climate Change. Cambridge, UK and New York, NY, USA: Cambridge University Press, pp. 1513–1766. https://doi.org/10.1017/9781009157896.013

Sievers, M., Brown, C.J., Mcgowan, J., Turschwell, M.P., Buelow, C.A., Holgate, B., et al. (2023) Co-occurrence of biodiversity, carbon storage, coastal protection, and fish and invertebrate production to inform global mangrove conservation planning. *Science of the Total Environment*, 904, 166357. Available from: https://doi.org/10.1016/j.scitotenv.2023.166357

Swales, A., Bentley, S.J., Sr. & Lovelock, C.E. (2015) Mangrove-forest evolution in a sediment-rich estuarine system: opportunists or agents of geomorphic change? *Earth Surface Processes and Landforms*, 40(12), 1672–1687. Available from: https://doi.org/10.1002/esp.3759

Thieler, E.R., Himmelstoss, E.A., Zichichi, J.L. & Ergul, A. (2009) The Digital Shoreline Analysis System (DSAS) version 4.0-an ArcGIS extension for calculating shoreline change (No. 2008-1278). US Geological Survey. https://doi.org/10.3133/ofr20081278

Thom, B.G. (1967) Mangrove ecology and deltaic geomorphology: Tabasco, Mexico. *Joural of Ecology*, 55, 301e343.

Toorman, E.A., Anthony, E., Augustinus, P.G., Gardel, A., Gratiot, N., Homenauth, O. et al. (2018) Interaction of mangroves, coastal hydrodynamics, and morphodynamics along the coastal fringes of the Guianas. *Threats to mangrove forests: hazards, vulnerability, and management*, pp.429–473. https://doi.org/10.1007/978-3-319-73016-5_20

Tran, T.V., Reef, R. & Zhu, X. (2022) A review of spectral indices for mangrove remote sensing. *Remote Sensing*, 14(19), 4868. Available from: https://doi.org/10.3390/rs14194868-

Vaughn, S.E. (2018) The political economy of regions: climate change and dams in Guyana. *Radical History Review*, 2018, 105–125. Available from: https://doi.org/10.1215/01636545-4355157

Veverka, L., Forinash, E., Roddom, E., Susanto Astra, A., Christ, B., Díazgranados, M.C., et al. (2025) Capacity building and connecting practitioners through the global mangrove Alliance. *Oceanography*, 38(1), 101–102. Available from: https://doi.org/10.5670/oceanog.2025.114

Vos, K., Splinter, K.D. & Palomar-Vázquez, J. (2023) Benchmarking satellite-derived shoreline mapping algorithms. *Communications Earth & Environment*, 4, 345. Available from: https://doi.org/10.1038/s43247-023-01001-2

Vousdoukas, M.I., Ranasinghe, R., Mentaschi, L., Plomaritis, T., Athanasiou, P., Luijendijk, A., et al. (2020) Sandy coastlines under threat of erosion. *Nature Climate Change*, 10, 260–263. Available from: https://doi.org/10.1038/s41558-020-0697-0

Walcker, R., Anthony, E.J., Cassou, C., Aller, R.C., Gardel, A., Proisy, C., et al. (2015) Fluctuations in the extent of mangroves driven by multidecadal changes in North Atlantic waves. *Journal of Biogeography*, 42, 2209–2219. Available from: https://doi.org/10.1111/jbi.12580

Winterwerp, J.C., De Graaff, R.F., Groeneweg, J. & Luijendijk, A.P. (2007) Modelling of wave damping at Guyana mud coast. *Coastal Engineering*, 54(3), 249–261. Available from: https://doi.org/10.1016/j.coastaleng.2006.08.012

Zhu, S., Wei, W., Zhu, Q., Wan, K., Xing, F., Yan, W., et al. (2024) Wave attenuation and transformation across a highly turbid muddy tidal flat-salt marsh system. *Applied Ocean Research*, 147, 103980. Available from: https://doi.org/10.1016/j.apor.2024.103980

Zu Ermgassen, P.S., Mukherjee, N., Worthington, T.A., Acosta, A., da Rocha Araujo, A.R., Beitl, C.M., et al. (2020) Fishers who rely on mangroves: modelling and mapping the global intensity of mangrove-associated fisheries. *Estuarine, Coastal and Shelf Science*, 247, 106975. Available from: https://doi.org/10.1016/j.ecss.2020.106975

SUPPORTING INFORMATION

Additional supporting information can be found online in the Supporting Information section at the end of this article.

How to cite this article: Rogers, M.S.J. & Spencer, T. (2026) Holistic analysis of shoreline change and mudbank dynamics across the Guiana coastline. *Earth Surface Processes and Landforms*, 51(7), e70351. Available from: https://doi.org/10.1002/esp.70351